A CD317/tetherin–RICH2 complex plays a critical role in the organization of the subapical actin cytoskeleton in polarized epithelial cells

Ruth Rollason, Viktor Korolchuk, Clare Hamilton, Mark Jepson, and George Banting

Department of Biochemistry, University of Bristol, Bristol BS8 1TD, England, UK

CD317/tetherin is a lipid raft–associated integral membrane protein with a novel topology. It has a short N-terminal cytosolic domain, a conventional transmembrane domain, and a C-terminal glycosyl-phosphatidylinositol anchor. We now show that CD317 is expressed at the apical surface of polarized epithelial cells, where it interacts indirectly with the underlying actin cytoskeleton. CD317 is linked to the apical actin network via the proteins RICH2, EBP50, and ezrin. Knocking down expression of either CD317 or RICH2 gives rise to the same phenotype: a loss of the apical actin network with concomitant loss of apical microvilli, an increase in actin bundles at the basal surface, and a reduction in cell height without any loss of tight junctions, transepithelial resistance, or the polarized targeting of apical and basolateral membrane proteins. Thus, CD317 provides a physical link between lipid rafts and the apical actin network in polarized epithelial cells and is crucial for the maintenance of microvilli in such cells.

Introduction

CD317, also known as BST2 or HM1.24 antigen (Goto et al., 1994; Vidal-Laliena et al., 2005) and recently designated tetherin (Neil et al., 2008), is an integral membrane protein with a novel topology. It has a conventional transmembrane domain (near its N terminus) and a C-terminal glycosyl-phosphatidylinositol (GPI) anchor (Kupzig et al., 2003). CD317 plays a role in regulating the growth and development of B cells and is highly expressed in human myeloma cells (Goto et al., 1994; Ishikawa et al., 1995; Ohtomo et al., 1999); its expression is up-regulated by interferon-α (Blasius et al., 2006), and it causes retention of fully formed HIV viral particles at the surface of HIV-infected cells (Neil et al., 2008; Van Damme et al., 2008).

CD317 was initially described as being present at the cell surface (Goto et al., 1994; Ishikawa et al., 1995; Ohtomo et al., 1999), but we subsequently demonstrated that it also resides in an intracellular pool and that it cycles between this intracellular pool and the cell surface (Kupzig et al., 2003), the internalization step being clathrin dependent (Rollason et al., 2007). CD317 resides, at least at the cell surface, in cholesterol-rich lipid microdomains (lipid rafts) with the transmembrane domain apparently lying outside the lipid raft and with the raft localization being dependent on its GPI anchor (Kupzig et al., 2003). Lipid rafts have been implicated as being important in membrane trafficking by helping to segregate proteins for delivery to specific locations and in cell signaling by providing platforms for the transient assembly of signaling complexes (for reviews see Simons and Toomre, 2000; Viola and Gupta, 2007). A recent review (Viola and Gupta, 2007) prefers the term "membrane rafts" to lipid rafts and defines membrane rafts as "small (10–200 nm in diameter), heterogenous, highly dynamic, sterol- and sphingolipid-enriched domains that compartmentalize cellular processes." Viola and Gupta (2007) highlight the fact that there have been several studies of integral membrane proteins that tether membrane rafts to the underlying actin cytoskeleton. Indeed, the work of Kusumi et al. (2005) has developed the "picket fence" model, originally proposed by Sheetz (1983), in which specific integral membrane proteins are linked to the actin cytoskeleton and thereby act as rows of pickets in the plane of the lipid bilayer, limiting the free diffusion of membrane lipids and proteins and thereby serving to establish highly dynamic

Correspondence to George Banting: g.banting@bristol.ac.uk

Abbreviations used in this paper: BAR, Bin/amphiphysin/Rvs; ERM, ezrin-radixin-moesin; GAP, GTPase-activating protein; GPI, glycosyl-phosphatidylinositol; LB, Luria Bertani; MLC, myosin light chain; PDZ, PSD-95/DlgA/ZO-1 like; ROCK, Rho kinase; SEM, scanning EM.

The Rockefeller University Press $30.00
J. Cell Biol. Vol. 184 No. 5 721–736
www.jcb.org/cgi/doi/10.1083/jcb.200804154

membrane microdomains. This linking of integral membrane protein "pickets" to the actin "fence" not only generates membrane microdomains, it also ensures proximity of the actin cytoskeleton to the region of the plasma membrane containing the membrane protein pickets, thereby intimately coupling the architecture of the cytoskeleton with that of the plasma membrane. Consistent with this model is the fact that a growing number of integral membrane proteins have been shown to be linked to the actin cytoskeleton, often via a member of the ezrin-radixin-moesin (ERM) family of proteins (Fanning and Anderson, 1999; Bretscher et al., 2000).

We have previously suggested that CD317 resides in the plasma membrane with its GPI anchor in a membrane raft and its transmembrane domain outside of the raft (or at the interface of the raft and nonraft domains; Kupzig et al., 2003). This would place the N-terminal cytosolic domain of CD317 in a suitable position to interact with the actin cytoskeleton. Therefore, we thought it appropriate to test whether CD317 does interact with the actin cytoskeleton.

In this study, we show that CD317 does interact, indirectly, with the actin cytoskeleton and that it plays a critical role in the organization of the actin cytoskeleton in polarized epithelial cells.

Results

CD317 localization in nonpolarized and polarized Caco-2 cells

We initially chose to determine the localization of CD317 in nonpolarized Caco-2 cells because we subsequently planned to investigate the possible role of CD317 in apical trafficking in polarized epithelia. Caco-2 cells are a good model for such experiments because, when they are grown at confluency on permeable filters for an extended duration (~2 wk), they differentiate into highly polarized monolayers with attributes similar to those of intestinal epithelial cells (Grasset et al., 1984). These include a tall, columnar morphology and tightly packed microvilli. Caco-2 cells can also be grown as nonpolarized cells on plastic or glass. We found that some CD317 is expressed at the surface of nonpolarized Caco-2 cells, but the majority is intracellular, which is a distribution similar to that previously described for rat, mouse, and human CD317 in nonpolarized cells (Kupzig et al., 2003; Blasius et al., 2006; Neil et al., 2008; Van Damme et al., 2008). However, in fully polarized Caco-2 cells, the predominant localization of CD317 is at the apical plasma membrane (Fig. 1 A).

CD317 knockdown

The fact that CD317 is apically localized in polarized Caco-2 cells suggested that it might play a role in the establishment or maintenance of the polarized phenotype. We chose to address this possibility by knocking down expression of CD317 using siRNA and then assaying whether this had any effect on the morphology of nonpolarized and polarized Caco-2 cells. CD317 expression was initially knocked down in nonpolarized Caco-2 cells using a plasmid-based siRNA expression system (see Materials and methods). Two different siRNA sequences (see Materials and methods) gave similar results. Stably transfected Caco-2 cells were selected and processed for immunofluorescence and immunoblot analysis using antibodies to CD317. This demonstrated that levels of CD317 expression had been reduced in the knockdown cells to <20% of those in control cells (Fig. 1 B and Fig. S1 A, available at http://www.jcb.org/cgi/content/full/jcb.200804154/DC1).

Colonies of nonpolarized Caco-2 cells in which CD317 expression had been knocked down appeared to have a subtly different phenotype to that seen in colonies of control cells. This led us to investigate the organization of the actin cytoskeleton in the CD317 knockdown cells. Colonies of CD317 knockdown cells were shown to possess significantly more-pronounced bundles of F-actin than control colonies as well as distinct filopodia at the periphery of colonies (Fig. 1 C). Immunoblot analysis of the total actin present in control and CD317 knockdown cells demonstrated that this extra F-actin is not the result of overexpression of actin (unpublished data) and is therefore most likely the result of increased F-actin polymerization.

CD317 knockdown in polarized Caco-2 cells

The fact that reducing expression of CD317 in nonpolarized Caco-2 cells results in an alteration in the organization of the actin cytoskeleton in those cells led us to ask what effect the reduced expression of CD317 would have on the phenotype of polarized Caco-2 cells (assuming they were still able to polarize after CD317 knockdown). Control Caco-2 cells were grown to confluency and allowed to polarize (as described in Materials and methods). As expected for polarized epithelial cells, the majority of the F-actin in these cells can be seen to be subapical (Fig. 2 A). CD317 knockdown Caco-2 cells grown to confluency also polarized and exhibited a similar gross morphology to that of control cells. However, there is a significantly different distribution of F-actin in these cells, with an almost complete absence of any detectable subapical F-actin and a preponderance of F-actin bundles at the basal membrane (Fig. 2 A). This observation suggested that knockdown of expression of CD317 might affect the organization of apical microvilli in polarized Caco-2 cells because F-actin fibers normally run along the length of microvilli providing mechanical support (Bretscher, 1991; Bartles, 2000). Scanning EM (SEM) analysis of polarized Caco-2 cells showed that although there is a dense network of long apical microvilli on the surface of control cells, the apical surface of CD317 knockdown cells is almost completely devoid of any microvilli; those that are present are sparse, short, and/or stubby (Fig. 2 A, right). XZ reconstructions of confocal images of control and CD317 knockdown cells show the altered distribution of F-actin and also that the knockdown cells appear to be shorter than their control counterparts (Fig. 2 A, middle). Measurement of the height of the monolayers shows that the knockdown cells are 5.6 ± 0.37 µm tall (n = 50), as opposed to 13.47 ± 0.9 µm (n = 50) for the control cells.

The formation of tight junctions between adjacent cells is an integral part of the normal process by which polarized monolayers of epithelial cells are formed (Yeaman et al., 1999). The observed differences in F-actin distribution and in cell height

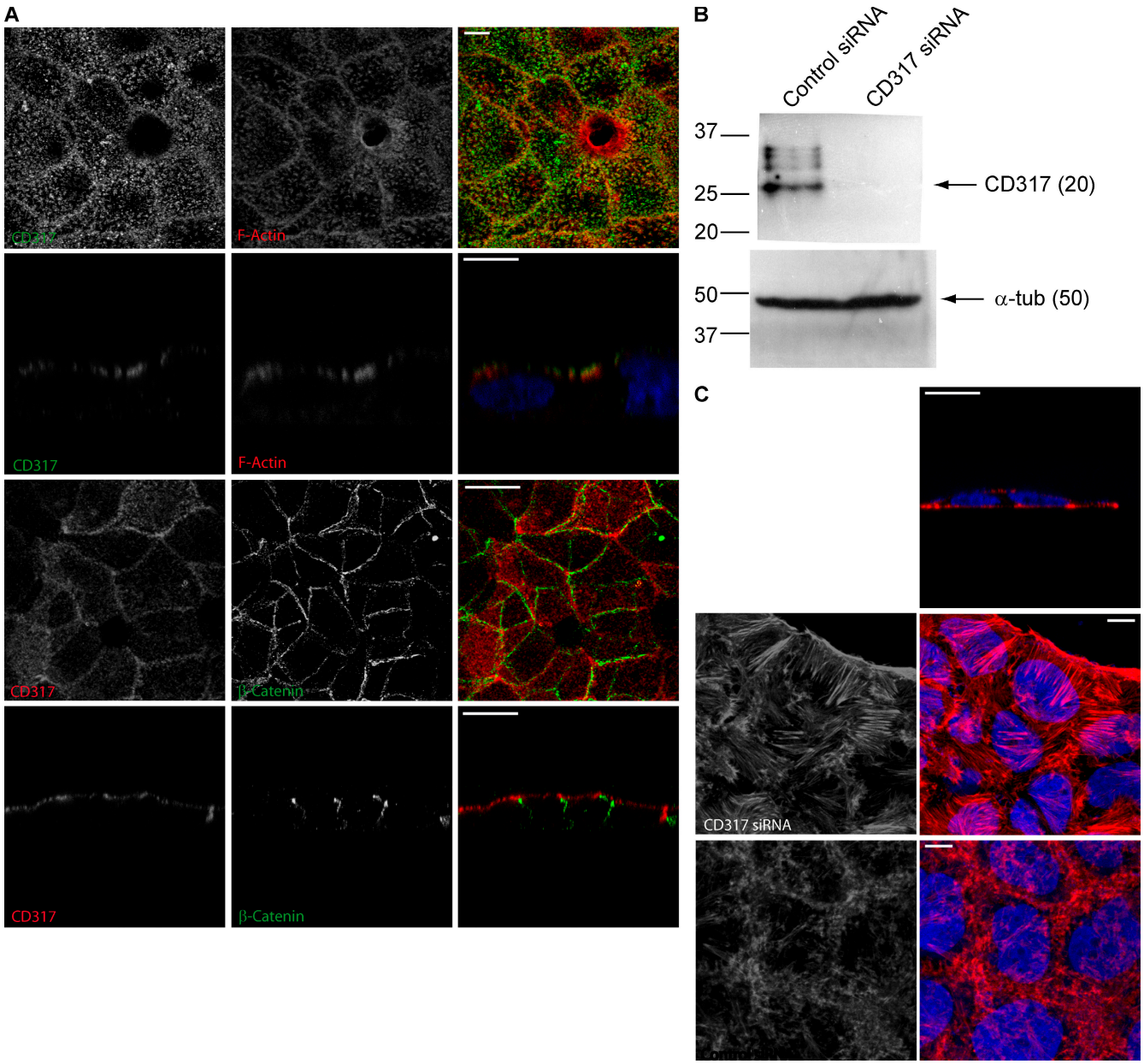

Figure 1. **Localization of CD317 in polarized Caco-2 cells, its knockdown in Caco-2 cells, and the effect of knockdown on F-actin.** (A) Localization of CD317 in polarized Caco-2 cells. The top row shows XY images of CD317 (detected with an anti-CD317 antibody) and F-actin (Alexa Fluor 594–phalloidin) localization as indicated. The second row shows an XZ section from the first row. The third row shows XY images of CD317 and β-catenin localization as indicated (β-catenin is a marker of lateral membranes). The bottom row shows an XZ section from the third row. Panels on the right show merged images of the left and middle panels, with DAPI-stained nuclei on the right in the second row. (B) Immunoblot analysis (using an anti-CD317 antibody) of lysates from Caco-2 cells stably expressing CD317 siRNA or control GFP siRNA as indicated. The bands representing higher molecular weight proteins in the control siRNA lane correspond to glycosylated CD317. An immunoblot of α-tubulin was used as a loading control. Molecular mass is indicated in kilodaltons. (C) Alexa Fluor 594–phalloidin decoration of F-actin in nonpolarized CD317 knockdown cells (top) and control cells (bottom). Each image shows a colony of cells with DAPI-stained nuclei. The top panel is an XZ section from a field of CD317 knockdown cells. Bars, 10 μm.

between control cells and CD317 knockdown cells led us to question whether tight junctions were forming correctly in the CD317 knockdown cells. Several assays were performed to address this question. First, confluent monolayers of CD317 knockdown and control cells were grown on permeable membrane supports. The transepithelial resistance was then measured and was consistently found to be 150–170 Ohm/cm^2 ($n > 20$) in both control and CD317 knockdown cell monolayers. These data suggested that tight junctions are still present, intact, and functional in the CD317 knockdown cells. As a further test of the integrity of the epithelial monolayer formed by CD317 knockdown cells, apical surface proteins were biotinylated in control and CD317 knockdown cells. Tight junctions are impermeable to biotin (Sargiacomo et al., 1989); so, if tight junctions are intact and functional, only apical membrane proteins should be biotinylated when the apical surface is labeled with biotin.

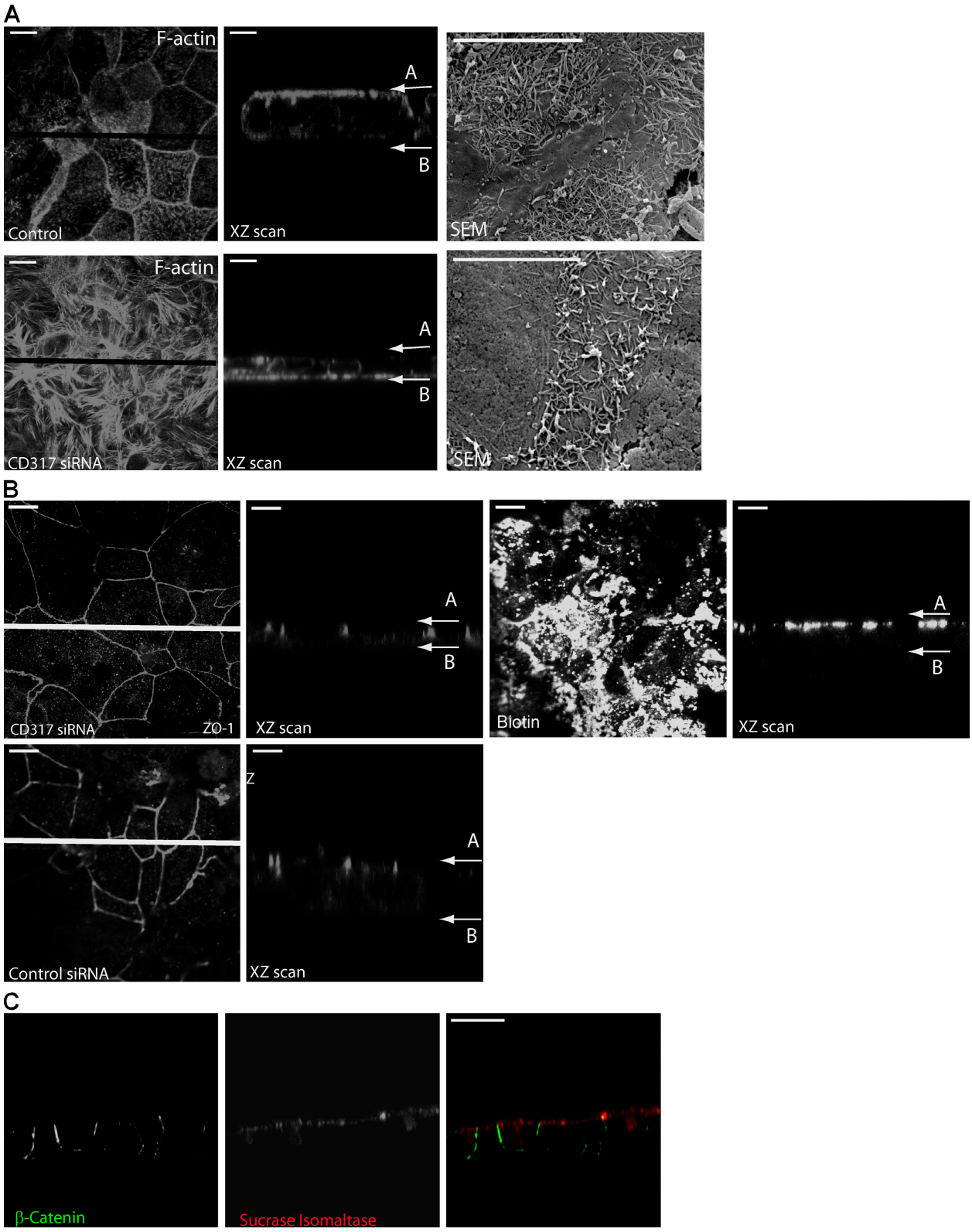

Figure 2. **The effect of CD317 knockdown in polarized Caco-2 cells.** (A) Left panels are maximum intensity projection XY images showing Alexa Fluor 594–phalloidin decoration of F-actin in polarized control and CD317 knockdown Caco-2 cells. Middle panels show XZ sections taken along the lines in left panels. Right panels show corresponding SEM images of the surface of control and CD317 knockdown cells. Arrows indicate the positions of the top (A) and bottom (B) of the cell monolayer. (B) ZO-1 labeling of tight junctions in polarized CD317 knockdown and control Caco-2 cells and biotin labeling of proteins in the apical membrane of polarized CD317 knockdown Caco-2 cells as indicated. Left panels are maximum intensity projection XY images, and right panels are XZ sections taken along the lines in the left panels. Arrows indicate the positions of the top (A) and bottom (B) of the cell monolayer. (C) Detection of β-catenin in the lateral membranes and sucrase-isomaltase in the apical membrane of polarized CD317 knockdown Caco-2 cells. XZ sections derived from maximum intensity projection XY images are presented. The right panel is a merge of the left and middle images. Bars, 10 μm.

This was what we observed in both control and knockdown cells (Fig. 2 B). In addition, immunolabeling of ZO-1, a component of tight junctions (Stevenson et al., 1986), clearly shows that it is present (and appropriately localized) in the knockdown cells (Fig. 2 B). Thus, tight junctions appear to be present and functional in monolayers of the polarized CD317 knockdown cells despite the major rearrangements in the actin cytoskeleton. Furthermore, markers of the lateral membrane (β-catenin; Toye et al., 2008) and apical membrane (sucrase-isomaltase; Hauri, 1985) are correctly localized in CD317 knockdown polarized cell monolayers (Fig. 2 C).

The knockdown phenotype can be rescued by expression of rat CD317

To show that the effect on the actin cytoskeleton arising as a result of the expression of CD317 siRNA is caused by the reduced expression of CD317 (and not caused by an off-target effect), we chose to attempt to rescue the normal phenotype by expression of the rat orthologue of human CD317 in the CD317 knockdown Caco-2 cells. Rat CD317-GFP is efficiently expressed and targeted to the apical membrane in polarized Caco-2 CD317 knockdown cells (Fig. S1, B and C). We observed that CD317 knockdown cells stably expressing rat CD317-GFP and polarized on permeable membrane supports have the same distribution of F-actin as that observed in control cells (i.e., bundles of basally localized F-actin are lost, and the F-actin is predominantly apically localized; Fig. S1 C).

The effects of CD317 knockdown are dependent on Rac and Rho

Activation of the small GTPases Rho and Rac leads to the formation of actin bundles/fibers, although the Rac-induced fibers are also Rho dependent (Ridley and Hall, 1992; Ridley et al., 1992). Therefore, we hypothesized that the actin bundles observed in CD317 knockdown cells might arise as a result of Rac and/or Rho activity and reasoned that if this were the case, transient expression of dominant-negative Rac in the CD317 knockdown cells should abrogate the knockdown phenotype (i.e., the actin bundles observed in the knockdown cells should be lost). This is what we observed; transient expression of a dominant-negative myc-tagged Rac mutant (Rac T17N) inhibits the formation of the characteristic F-actin structures seen in the CD317 knockdown cells (76.75% of cells expressing Rac T17N had reduced or no actin bundles; $n = 83$; Fig. 3 A), whereas transient expression of a dominant-negative cdc42 mutant does not (77% of cells expressing dominant-negative cdc42 showed no change in the degree of actin bundling; $n = 23$; Fig. 3 A). Furthermore, as would be expected, incubation of CD317 knockdown cells in the presence of 1 μM of the Rho kinase (ROCK) inhibitor Y-27632 for 30 min also leads to loss of these structures (Fig. 3 A).

Further consequences of Rho activation are the phosphorylation on Ser19 of myosin light chain (MLC) by ROCK (Amano et al., 1996) and inactivation of MLC phosphatase (Tapon and Hall, 1997). Changes in the Ser19 phosphorylation status of MLC can thus be used as a biochemical readout of Rho activation. We observed that the amount of Ser19-phosphorylated MLC in CD317 knockdown cells is >10-fold that detected in control cells (control cells were untransfected Caco-2 cells, lamin A/C knockdown Caco-2 cells, or CD317 knockdown Caco-2 cells rescued by expression of rat CD317; Fig. 3 B and Fig. S2 A, available at http://www.jcb.org/cgi/content/full/jcb.200804154/DC1). These biochemical data are consistent with the observed phenotype and implicate CD317 in aspects of the regulation of Rac and Rho function in Caco-2 cells. However, they do not provide direct evidence that there is an increase in the level of active Rac in CD317 knockdown cells. To address this directly, we performed a pull-down assay for active Rac (see Materials and methods) using lysate from polarized Caco-2 cells (control lamin A/C knockdown, CD317 knockdown, and rescued CD317 knockdown). This demonstrated an increase in the amount of active Rac in CD317 knockdown cells compared with that in either control or rescued cells, with levels of active Rac being barely detectable in the control and rescued cells (Fig. 3 C and Fig. S2 B). Thus, there is an increase in the level of active Rac in polarized Caco-2 CD317 knockdown cells.

Ezrin is mislocalized in CD317 knockdown cells

Given that knocking down expression of CD317 in polarized Caco-2 cells leads to a loss of apical microvilli and a change in the regulation of Rho activity, we speculated that ERM proteins might be mislocalized in CD317 knockdown cells. Members of the ERM family of closely related proteins function as cross-linkers between the plasma membrane and actin filaments (Bretscher et al., 2000, 2002), and such cross-links are fundamental to the making and maintenance of microvilli (Yonemura et al., 1999; Saotome et al., 2004; Hanono et al., 2006). Soluble ERM proteins in the cytosol are inactive in terms of their cross-linking activity (Pearson et al., 2000), but when ERM proteins are activated (involving phosphorylation), they undergo a conformational change that allows them to interact with both actin and, directly or indirectly, with the cytosolic domains of specific integral membrane proteins (Bretscher et al., 2000, 2002). Rho activity has also been implicated in the activation of ERM proteins (Bretscher et al., 2000). Because ezrin is normally enriched in apical microvilli in polarized epithelial cells, where it plays a critical role in coupling the actin cytoskeleton to the plasma membrane (Bretscher, 1983; Berryman, 1993), we reasoned that it would be mislocalized in CD317 knockdown cells lacking apical microvilli. As expected, we observed that ezrin localizes to the apical membrane in control polarized Caco-2 cells where there is some colocalization with F-actin (Fig. 3 D, top). However, in CD317 knockdown cells, this is not the case (Fig. 3 D, bottom). It is noteworthy that phosphorylation of ezrin is raised threefold in knockdown cells compared with control cells (both lamin A/C knockdown and rescued CD317 knockdown; Fig. 3 E and Fig. S3 B, available at http://www.jcb.org/cgi/content/full/jcb.200804154/DC1), implying that the block on the formation of microvilli is not at the level of ezrin activation. These data also demonstrate that reexpression of CD317 in the knockdown cells restores the level of ezrin phosphorylation to that seen in control cells.

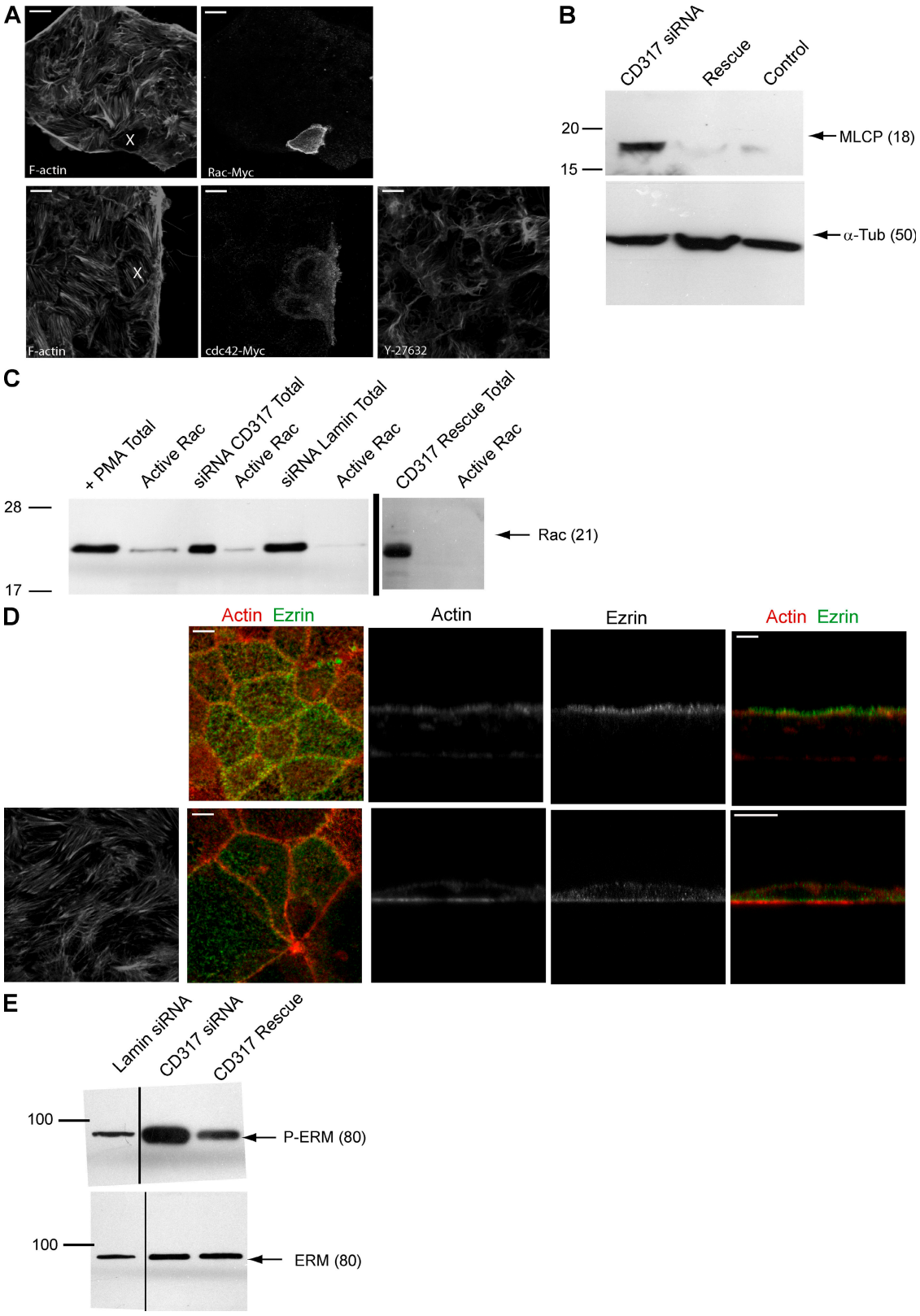

Figure 3. **CD317 knockdown leads to activation of Rac.** (A) Alexa Fluor 594–phalloidin decoration of F-actin in nonpolarized CD317 knockdown Caco-2 cells transiently expressing either dominant-negative myc-tagged Rac or dominant-negative myc-tagged cdc42 as indicated (x = transfected cells) or after incubation of cells with the ROCK inhibitor Y-27632 as indicated. (B) Immunoblot analysis of phosphorylated Ser19 of MLC (MLCP) in lysates from CD317 knockdown, CD317 rescue, and control Caco-2 cells. An immunoblot of α-tubulin was used as a loading control. (C) Results of pull-down assay for active Rac showing an immunoblot of Rac detected with an anti-Rac antibody. The left lane of each pair shows the total amount of Rac present in 10% of the lysate used in the assay. The right lane of each pair shows the active Rac isolated in the pull-down in each case. Lysates were from the indicated polarized Caco-2 cells. Lysates from PMA-treated cells were used as a positive control for the presence of active Rac. (D) Ezrin and F-actin localization in

CD317 interacts with RICH2, a protein with both a Bin/amphiphysin/Rvs (BAR) and Rho GTPase-activating protein (GAP) domain

Having shown that knockdown of CD317 expression leads to a change in organization of the actin cytoskeleton and a concomitant change in localization of ezrin and having implicated Rac and Rho activity in this phenotype, we reasoned that there might be some physical link between CD317 and ezrin and/or Rac and/or Rho or possibly with the actin cytoskeleton itself. Therefore, we chose to screen for proteins that interact with the cytosolic domain of CD317. Our chosen strategy was to use a synthetic peptide, corresponding to the cytosolic domain of CD317 and tethered to a matrix support at its C terminus, to screen a bacteriophage display library (see Materials and methods). The rationale for screening a bacteriophage display library rather than a yeast two-hybrid library was that we reasoned that any interaction with the cytosolic domain of CD317 might require the free N terminus of CD317; this would be blocked by fusion to the yeast partner protein in any yeast two-hybrid bait construct but would remain exposed in the C-terminally tethered peptide that was used to screen the bacteriophage display library. The screen identified 19 sequences encoding potential interactors. This included several proteins we considered to be improbable genuine interactors with CD317 (e.g., hypothetical proteins and ribosomal proteins; Fig. S2 D). However, one protein identified as a candidate interactor was RICH2 (Richnau and Aspenstrom, 2001). Several features of RICH2 (see the next paragraph) suggested that it might be a genuine interactor with the CD317 cytosolic domain. Therefore, we used three further techniques to confirm the CD317–RICH2 interaction. The first was a pull-down assay in which a synthetic peptide, biotinylated at its C terminus and corresponding to the entire cytosolic N terminus of CD317, was immobilized on streptavidin-coated beads and used to isolate a fusion protein of the C-terminal 87 amino acids of RICH2 fused to GST (Fig. 4 A). Biotin-coated beads did not bind the GST-RICH2 fusion (Fig. 4 A), and GST did not bind to the beads coated with the CD317 peptide. The second technique was coimmunoprecipitation. In initial experiments, CD317-GFP was immunoprecipitated using an anti-GFP antibody from COS cells expressing CD317-GFP and RICH2-RFP, and the immunoprecipitated material was probed with an antibody to RICH2 (Fig. 4 B, top). In subsequent experiments, endogenous CD317 was immunoprecipitated from polarized Caco-2 cells (or CD317 knockdown Caco-2 cells), and the immunoprecipitated material was probed with an antibody to RICH2 (Fig. 4 B, bottom). RICH2 was detected in material isolated from control cells but not from that isolated from the CD317 knockdown cells, demonstrating that endogenous RICH2 interacts with endogenous CD317. The third technique used to confirm the CD317–RICH2 interaction was surface plasmon resonance. The biotinylated synthetic peptide corresponding to the cytosolic N terminus of CD317 was immobilized on a streptavidin-coated gold chip, and the GST-RICH2 fusion protein passed over the chip at different concentrations. The GST-RICH2 fusion protein can be seen to bind to the immobilized CD317 peptide in a dose-responsive manner (Fig. 4 C). Thus, all three techniques confirmed that RICH2 interacts with the cytosolic domain of CD317, and experiments using the GST-RICH2 fusion demonstrate that the C-terminal 87 amino acids of RICH2 are involved in that interaction.

RICH2 was originally identified as a homologue of RICH1 (also known as Nadrin [Harada et al., 2000] and ARHGAP17 [Katoh and Katoh, 2004]; Richnau and Aspenstrom, 2001). RICH2, different isoforms of RICH1, and related proteins share two conserved domains, namely an N-terminal BAR domain and a Rho/Rac/cdc42 GAP domain (Richnau and Aspenstrom, 2001; Furuta et al., 2002). These domains are followed by a variable (in sequence and length) region (Fig. 4 D). However, RICH2 and isoforms 1 and 2 of RICH1 do share the same C-terminal sequence Glu-Ser-Thr-Ala-Leu (ESTAL), which conforms to a PSD-95/DlgA/ZO-1–like (PDZ) domain–binding motif (Songyang et al., 1993) and has been implicated in binding to the protein EBP50 (ERM-binding phosphoprotein 50; also known as NHERF1 [Na^+/H^+ exchanger regulatory factor 1]; Reczek and Bretscher, 2001). EBP50 (Weinman et al., 1995) is a PDZ domain–containing adapter that has been shown to link ERM proteins with the cytosolic domains of specific integral membrane proteins (Bretscher et al., 2000). In this case, RICH2 appears to provide a physical link between the cytosolic domain of CD317 and EBP50 and thus to ezrin and the actin cytoskeleton. We reasoned that if this were the case, it should be possible to coimmunoprecipitate EBP50 with CD317. We immunoprecipitated CD317 from lysate from polarized Caco-2 cells (control or CD317 knockdown) and immunoblotted the immunoprecipitates using an anti-EBP50 antibody. EBP50 was detectable in the immunoprecipitate from control cells but not in that from CD317 knockdown cells (Fig. 4 E and Fig. S2 C).

RICH2 also appears to provide a potential link between CD317 and regulation of Rac and Rho because the central putative GAP domain has been shown to have Rac GAP activity in vitro (Richnau and Aspenstrom, 2001).

The BAR domain of RICH2 has been shown to bind membranes and to be capable of inducing membrane tubulation (Richnau et al., 2004). Consistent with this in vitro observation, we found RICH2 to be present in the membrane fraction from Caco-2 cells after the separation of membrane and cytosol fractions (Fig. 4 F). This was also the case for RICH2 in CD317 knockdown Caco-2 cells (unpublished data); thus, CD317 is not required for the membrane association of RICH2.

polarized control (top) and CD317 knockdown (bottom) Caco-2 cells. The left pair of images shows XY sections of the apical surface of the cell monolayer, and the remaining images represent XZ sections of the monolayer. The basal F-actin image (bottom left) shows an XY section of F-actin in the basal region of the polarized CD317 knockdown Caco-2 cells. (E) Immunoblot analysis of C-terminal Thr phosphorylation of ezrin in the indicated Caco-2 cell lysates. Immunoblot of total ezrin was used as a loading control. Black lines indicate that intervening lanes have been spliced out. (B, C, and E) Molecular mass is indicated in kilodaltons. Bars, 10 μm.

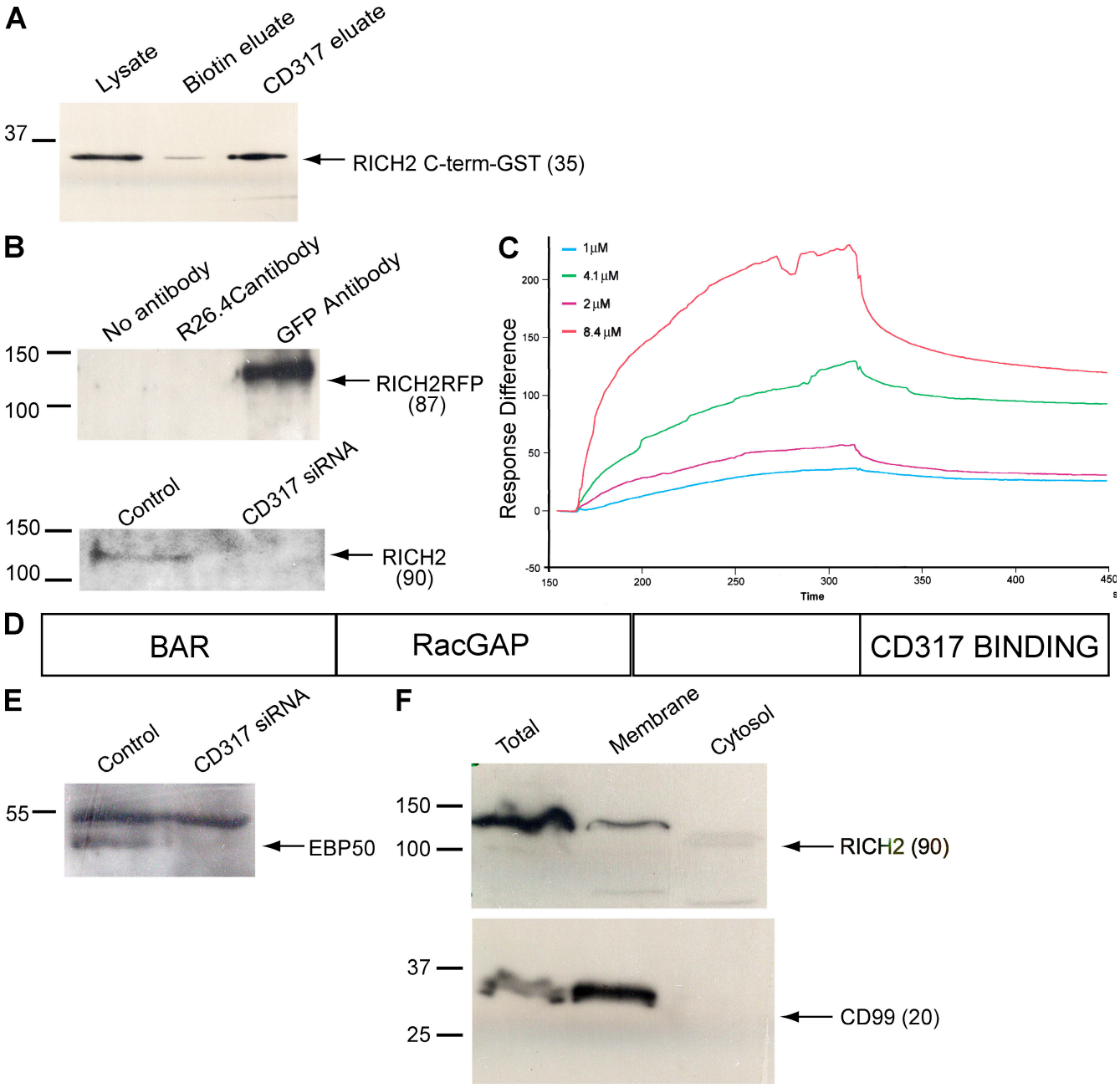

Figure 4. **CD317 interacts with RICH2.** (A) Immunoblot probed with an anti-RICH2 polyclonal antibody showing the results of a pull-down assay between a GST-RICH2 fusion protein and a synthetic peptide corresponding to the entire cytosolic N terminus of CD317. Lysate = 10% of total *E. coli* lysate used in the pull-down; Biotin eluate = GST-RICH2 eluted from biotin-coated beads; CD317 eluate = GST-RICH2 eluted from CD317 peptide-coated beads. (B, top) Immunoblot (using an anti-RICH2 antibody) of immunoprecipitates (using the indicated antibodies) from lysate of COS cells expressing CD317-GFP and RICH2-RFP (R26.4C antibody detects ZO-1 and was used as a control). (bottom) Immunoblot (using an anti-RICH2 antibody) of immunoprecipitates (generated using an anti-CD317 antibody) of lysate from polarized control Caco-2 cells or polarized CD317 knockdown Caco-2 cells as indicated. (C) Surface plasmon resonance data from an experiment in which the indicated concentrations of GST-RICH2 were flowed over a streptavidin-coated surface (flow channel) to which biotinylated CD317 N-terminal peptide had been attached. GST-RICH2 at the indicated concentrations was added at 160 s and stopped being added at 320 s. Data represent the binding of GST-RICH2 minus binding to a biotin-blocked control flow channel linked in series to the test channel. (D) Cartoon of the domain organization of RICH2. The region of RICH2 indicated as binding to CD317 was identified because this was the region detected in the initial bacteriophage display screen. The C terminus of RICH2 is a PDZ domain–binding motif, ESTAL. (E) Immunoblot (using an anti-EBP50 antibody) of material immunoprecipitated from lysates of polarized control Caco-2 cells and polarized CD317 knockdown Caco-2 cells (CD317 siRNA) using an anti-CD317 antibody. The top band present in both lanes corresponds to the heavy chain of the anti-CD317 antibody used in the immunoprecipitation. (F) Immunoblot analysis of membrane and cytosol fractions from Caco-2 cells using antibodies to RICH2 and the integral membrane protein CD99 as indicated. (A, B, E, and F) Molecular mass is indicated in kilodaltons.

RICH2 knockdown in Caco-2 cells leads to a similar phenotype to that arising after CD317 knockdown

We reasoned that if RICH2 does provide a functional link between CD317, Rac/Rho, and the actin cytoskeleton, knockdown of RICH2 expression should phenocopy knockdown of CD317 expression in Caco-2 cells. To test this hypothesis, the expression of RICH2 was knocked down in Caco-2 cells using the same plasmid-based method that was used to knock down expression of CD317 in these cells. Immunoblot analysis of lysate from control and RICH2 knockdown cells demonstrated that RICH2 levels in knockdown cells had been reduced to <20% of those detected in control cells (Fig. 5 A and Fig. S3 A). The stably transfected RICH2 knockdown Caco-2 cells were then grown to confluence to generate polarized monolayers. These polarized RICH2 knockdown cells phenocopy the polarized CD317 knockdown cells (i.e., a loss of apical F-actin, the presence of distinct bundles of F-actin at the basal membrane, a decrease in the amount of apically localized ezrin [Fig. 5 B], a loss of apical microvilli [Fig. 5 C], and reduced cell height but no loss of transepithelial resistance or of tight junctions or any change in the distribution of apical and basolateral marker proteins [not depicted]). Lamin A/C knockdown cells were used as a control in these experiments and showed a wild-type phenotype with respect to actin organization, microvilli formation, ezrin localization, and cell height. Knocking down expression of RICH2 also led to an increase in the level of active Rac in polarized Caco-2 cells (Fig. 5 D and Fig. S2 B), an ~10-fold increase in phosphorylation of MLC (Fig. 5 E and Fig. S2 A), and an approximately threefold increase in phosphorylated ezrin (when compared with the situation in control cells; Fig. 5 F and Fig. S3 B), closely paralleling what occurs when CD317 expression is knocked down.

The fact that RICH2 knockdown cells are phenocopies of CD317 knockdown cells is consistent with the two proteins acting on the same pathway, whereas the increase in MLC phosphorylation observed in RICH2 and CD317 knockdown cells is indicative of Rac and Rho activation in these cells. Rac and Rho activities have previously been shown to be required for production of actin-dependent ruffles (Hall, 1998). Therefore, we reasoned that if the putative Rac GAP domain in RICH2 is indeed functioning as a Rac GAP in vivo (as it has been shown to be in vitro; Richnau and Aspenstrom, 2001), elevated expression of RICH2 might lead to a reduction in active Rac within cells, which would, in turn, lead to a reduction in actin-dependent ruffles. To test this hypothesis, we expressed an RFP-tagged form of RICH2 (RICH2-RFP) in COS cells and assayed ruffle formation in these and in control, nontransfected cells. Over 90% of control cells exhibited ruffles, whereas <20% of cells expressing RICH2-RFP did so. An R288A mutation in the Rac GAP domain of RICH1 has previously been shown to destroy GAP activity in that protein (Richnau and Aspenstrom, 2001). Therefore, we generated the corresponding mutation (R291A) in RICH2-RFP and expressed the mutant protein in Caco-2 cells. Cells expressing R291A RICH2-RFP behaved as control cells, demonstrating that the Rac GAP activity of RICH2 is required to inhibit ruffle formation, which is a result consistent with the Rac GAP domain of RICH2 working as a Rac GAP in vivo.

RICH2 knockdown affects the localization of CD317

We considered that RICH2 might play a role in tethering CD317 at the apical membrane of polarized Caco-2 cells in much the same way that EBP50 and ezrin have been shown to tether the cystic fibrosis transmembrane conductance regulator in the apical membrane of polarized epithelial cells (Haggie et al., 2006). Therefore, we performed immunofluorescence analysis of the localization of endogenous CD317 in polarized RICH2 knockdown Caco-2 cells. Initial observations of XY images of methanol-fixed cells suggested that the majority of CD317 was still in the apical membrane in the RICH2 knockdown cells, but some appeared to be intracellular (Fig. 6, top left, arrows). Immunofluorescence analysis of PFA-fixed (nonpermeabilized) cells showed that CD317 is present at the apical plasma membrane (Fig. 6, second row). However, XZ images from methanol-fixed (permeabilized) polarized control and RICH2 knockdown cells (Fig. 6, third and fourth rows) clearly demonstrate an intracellular population of CD317 molecules in the RICH2 knockdown cells, which is a population of CD317 molecules that is not readily detectable in the control cells. This result implies that RICH2 is required to tether CD317 in the apical membrane.

Discussion

We have shown that knocking down expression of CD317 in Caco-2 cells does not prevent those cells from forming a polarized monolayer. Monolayers of CD317 knockdown Caco-2 cells have intact tight junctions and show appropriate localization of integral membrane protein markers of both apical and basolateral membranes. In these regards, they are no different than monolayers of polarized control cells. However, monolayers of CD317 knockdown Caco-2 cells do show significant differences to control cells when it comes to organization of the actin cytoskeleton. The knockdown cells show an almost complete loss of the well-defined and dense apical actin network. This network is of fundamental importance as the platform for the actin fibers that provide the mechanical support for the apical microvilli of polarized epithelial cells. We have also identified RICH2 as a membrane protein that interacts directly with the cytosolic domain of CD317 and can interact, via EBP50 and ezrin, with the actin cytoskeleton. The fact that knocking down expression of RICH2 has the same effects as knocking down expression of CD317 is consistent with RICH2 being part of the link between CD317 and the actin cytoskeleton. Thus, CD317 would seem to be acting like a "coat hanger" in the apical membrane of polarized cells with the actin cytoskeleton tethered to it via the RICH2/EBP50/ezrin linkage.

Clearly, CD317 is not simply acting as a coat hanger in the apical membrane; its presence in the apical membrane also has an effect on the activities of Rac and Rho. Therefore, it is noteworthy that RICH2 possesses a Rac GAP domain. This domain appears to be functional as a Rac GAP in cells because elevated expression of RICH2 leads to a loss of Rac-induced membrane ruffles, whereas a point mutation previously shown to block Rac GAP activity (Richnau and Aspenstrom, 2001) prevents RICH2 from having this effect. Furthermore, there are increased levels of active Rac in RICH2 knockdown cells. Thus,

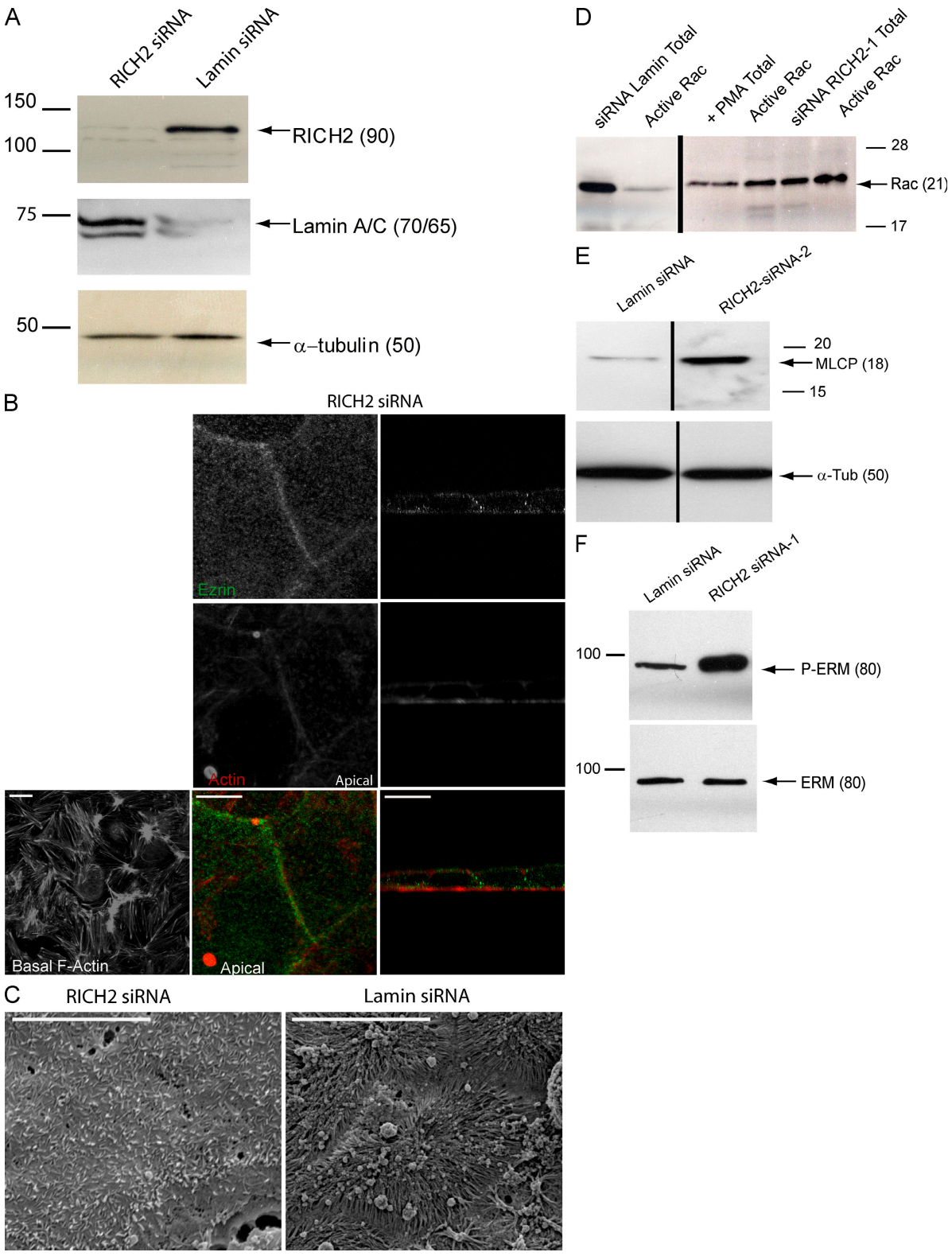

Figure 5. **Effects of RICH2 knockdown.** (A) Immunoblot analyses (using antibodies to RICH2 and lamin A/C) of lysates from Caco-2 cells in which either RICH2 or lamin A/C levels (as indicated) have been knocked down. An immunoblot of α-tubulin was used as a loading control. (B) Ezrin and F-actin localization in filter-grown polarized RICH2 knockdown Caco-2 cells. The actin basal panel shows an XY optical section of actin at the basal surface, and the actin apical panel shows the same at the apical surface of polarized RICH2 knockdown Caco-2 cells. The panel to the right of the actin apical image shows an XZ section of the same cells, highlighting the fact that F-actin is present at the basal membrane. (C) SEM of the apical surface of filter-grown polarized RICH2 and lamin A/C knockdown Caco-2 cells. (D) Results of pull-down assay for active Rac showing an immunoblot with Rac detected with an anti-Rac antibody. The left lane of each pair shows the total amount of Rac present in 10% of the lysate used in the assay. The right lane of each pair shows the active Rac isolated in the pull-down. Lysates were from the indicated polarized Caco-2 cells. Lysates from PMA-treated cells were used as a positive control for the presence of active Rac. (E) Immunoblot analysis of phosphorylated Ser19 of MLC (MLCP) in lysates from RICH2 knockdown or control lamin

in the case of polarized cells, one might speculate that the Rac GAP domain of RICH2 would lead to inactivation of any Rac molecules at the inner leaflet of the apical plasma membrane, thereby ensuring no Rac-dependent remodeling of the actin cytoskeleton at that location. It is noteworthy that the expression of constitutively active Rac has been shown to mediate the disintegration of microvilli in chemokine-activated T lymphocytes (Nijhara et al., 2004). Therefore, the inactivation of Rac by the RICH2 GAP domain would help to maintain integrity of the cortical actin network beneath the apical plasma membrane and would help to ensure retention of the actin fibers that give the mechanical support for the apical microvilli of polarized epithelial cells.

Others have shown that RICH1 can form a complex with a protein designated angiomotin and that this complex is important for the formation, maintenance, stability, and integrity of tight junctions in epithelial cells (Wells et al., 2006). Whereas we observed that tight junctions remain functional and intact after knockdown of RICH2 expression, knockdown of RICH1 expression led to a complete loss of tight junctions. Thus, RICH1 and RICH2 appear to play complementary roles in the establishment and maintenance of epithelial cell polarity.

Another cytosolic protein, EPI64 (EBP50-PDZ interactor of 64 kD), which binds EBP50 via a C-terminal DTYL motif and thereby links to the actin cytoskeleton via ezrin, plays a critical role in regulating the organization and structure of subdomains within epithelial microvilli (Hanono et al., 2006). Unlike RICH1 and RICH2, EP164 does not possess a BAR domain or a Rac/Rho/cdc42 GAP domain but has been shown to be a GAP for Rab27A (Itoh and Fukuda, 2006) and to bind Arf6-GTP, possibly protecting Arf6-GTP from inactivation by a GAP (Hanono et al., 2006). However, it is unclear how EP164 links to the plasma membrane. What is clear is that there is a growing number of partners for EBP50 that possess a GAP domain and one or more other protein or lipid interaction domain. Therefore, such proteins can provide part of a larger mechanical scaffold to localize specialized regions of the actin cytoskeleton while at the same time regulating the activity of specific small G proteins that play a role in trafficking pathways and/or the regulation of the local organization of the actin cytoskeleton.

The apical membranes of polarized epithelial cells are sphingolipid and cholesterol rich (Schuck and Simons, 2004). Given its previously demonstrated localization to membrane rafts, its possession of a GPI anchor, and the fact that it is N-glycosylated (Kupzig et al., 2003), it is perhaps not surprising that CD317 is localized to the apical membrane of polarized epithelial cells. However, clustering of GPI-anchored proteins may well be the most critical event in their apical delivery and localization (Hannan et al., 1993; Paladino et al., 2004; for review see Rodriguez-Boulan and Müsch, 2005). Whether CD317 plays any role in organizing membrane rafts in the apical membrane of polarized epithelial cells is unclear, but it is clear that CD317 has the potential to function as the type of picket proposed by Kusumi et al. (2005) linking through to the underlying fence of the actin cytoskeleton. Indeed, if CD317 is arranged as previously suggested (Kupzig et al., 2003), with the GPI anchor in a membrane raft and the transmembrane domain lying outside of the raft (or at the interface of raft and nonraft membrane), it might be considered to constitute a "tethered picket," with the GPI anchor being the tether holding the protein in the membrane raft. CD317 would thereby provide a mechanical link between membrane rafts and the actin cytoskeleton, a role not dissimilar to that previously proposed for the tetraspanin protein CD82 in T lymphocytes (Delaguillaumie et al., 2004). The recent designation of CD317 as tetherin, albeit for a totally different reason (Neil et al., 2008), would therefore seem entirely appropriate. Such a role for CD317/tetherin would be consistent with the observation that when GPI-anchored proteins arrive at the apical plasma membrane they are transiently immobilized (Hannan et al., 1993).

We have recently shown that, in nonpolarized cells, CD317 constitutively cycles between the cell surface and an intracellular compartment. Internalization from the cell surface is clathrin mediated and is dependent on the AP2 adapter complex; indeed, the cytosolic domain of CD317 interacts directly with the μ2 subunit of the AP2 adapter complex via an atypical dual tyrosine motif (Rollason et al., 2007). Furthermore, the cytosolic domain of CD317 also interacts directly with the μ1A subunit of the AP1 adapter complex, and this interaction is required to deliver the protein back to the TGN from an endocytic compartment (Rollason et al., 2007). An AP1 complex (AP1B), in which the μ1A subunit is replaced by a μ1B subunit, is specifically expressed in epithelial cells and has been shown to play a role in the delivery of cargo to the basolateral surface of polarized epithelial cells (Gravotta et al., 2007). This process is dependent on AP1B recognizing a motif, which is often Tyr based, in the cytosolic domain of cargo integral membrane proteins (Gravotta et al., 2007; Fölsch, 2008). However, adapters other than AP1B may also play a role in the recruitment of clathrin during the formation of transport intermediates involved in delivering proteins to the basolateral membrane (Deborde et al., 2008). Thus, because the cytosolic domain of CD317 possesses a Tyr motif that is recognized by AP1A in nonpolarized cells, one might have anticipated that it would be recognized by AP1B in polarized epithelial cells, leading to the delivery of CD317 to the basolateral surface of those cells. We have found no evidence for this, although it is of course possible that newly synthesized CD317 is initially delivered to the basolateral membrane before delivery to the apical membrane as has been shown to occur for some GPI-anchored proteins and some integral membrane proteins (for review see Rodriguez-Boulan and Müsch, 2005).

RICH2 interacts with the same region of the CD317 cytosolic domain that is recognized by μ1 and μ2. The interaction between the cytosolic domain of CD317 and RICH2 at the apical surface of polarized epithelial cells presumably masks the

knockdown Caco-2 cells. An immunoblot of α-tubulin was used as a loading control. (F) Immunoblot analysis of C-terminal Thr phosphorylation of ezrin in the indicated Caco-2 cell lysates. An immunoblot of total ezrin was used as a loading control. (D and E) Black lines indicate that intervening lanes have been spliced out. (A and D–F) Molecular mass is indicated in kilodaltons. Bars: (B) 10 μm; (C) 2 μm.

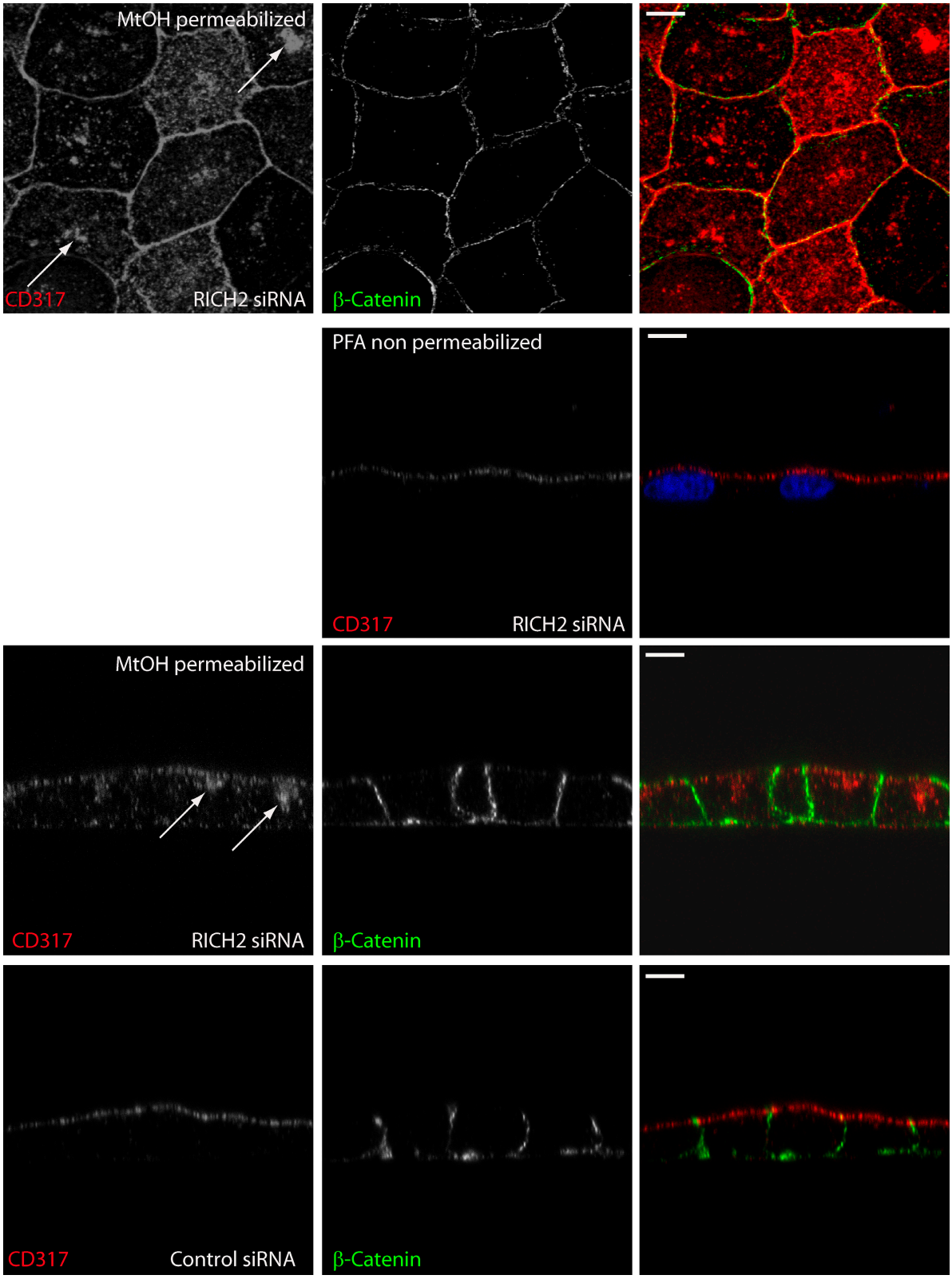

Figure 6. **RICH2 knockdown leads to a change in the localization of CD317.** Localization of CD317 in polarized RICH2 knockdown Caco-2 cells. The top row shows maximum intensity projection XY images of CD317 and β-catenin, as indicated, in methanol-fixed cells. Arrows indicate potential intracellular populations of CD317 molecules. The second row shows detection of CD317 in PFA-fixed (nonpermeabilized) cells (XZ sections); the right panel shows DAPI-stained nuclei in addition to the apical CD317. The third and fourth rows present XZ sections from methanol-fixed (permeabilized) cells showing CD317 and β-catenin localization in RICH2 knockdown and control polarized Caco-2 cells as indicated. Bars, 10 μm.

μ1/μ2-binding site on CD317, thereby preventing its internalization. This is consistent with our observation that CD317 is inefficiently internalized in polarized Caco-2 cells and that no intracellular pool of CD317 can be detected in polarized Caco-2 cells. It is also consistent with our observation that an intracellular pool of CD317 can be detected in RICH2 knockdown cells (this may well be because, in the absence of RICH2, μ2 can bind to the cytosolic domain of CD317 and bring about endocytosis of CD317).

CD317 clearly plays a critical role in the organization of the cytoskeleton in polarized epithelial cells. It will be interesting to see whether it plays a similar role in other cell types, notably B lymphocytes and other cells of the immune system in which it has been shown to be expressed and in which its level of expression is regulated by interferon-α (Goto et al., 1994; Ishikawa et al., 1995; Ohtomo et al., 1999; Blasius et al., 2006).

Materials and methods

Strains and culture conditions

Caco-2 and COS cells were maintained in DME (Invitrogen), 10% fetal calf serum, and 1% penicillin/streptomycin in a 5% CO_2 atmosphere at 37°C. Cells were polarized either by seeding at high density on coverslips or by seeding onto permeable filters (Thermo Fisher Scientific) and culturing for 14 d.

Plasmids and antibodies

Hairpin siRNA sequences 5′-CCAGGTCTTAAGCGTGAGA-3′ and 5′-TCGCGGACAAGAAGTACTA-3′ (corresponding to base pairs 432–450 and 452–470 of the human CD317 sequence, respectively), 5′-CAACATCCGATACTTGATA-3′ and 5′-TGCCAACTACAGCTCAATG-3′ (corresponding to base pairs 1,115–1,133 and 1,385–1,403 of the human RICH2 [KIAA0672] sequence, respectively), 5′-CTGGACTTCCAGAAGAACA-3′ (corresponding to base pairs 807–825 of the lamin A/C human sequence; Denti et al., 2004), and the control 5-GGTTATGTACAGGAACGCA-3′ (corresponding to the cycle 3 GFP [Invitrogen] sequence) were cloned into the pSilencer Hygro vector (Applied Biosystems). The rat CD317-GFP has been described previously (Kupzig et al., 2003), as have the dominant-negative RacN17 and cdc42N17 constructs, which were provided by G. Cory (University of Bristol, Bristol, England, UK; Coso et al., 1995). The RICH2-RFP construct was made by replacing the sequence between base pairs 1,331 and 2,190 of RICH2 with monomeric RFP. The A291 mutant was generated using the QuikChange Site-Directed Mutagenesis kit (Agilent Technologies) to change R291 for Ala. The CD317 antibodies used were HM1.24 mouse monoclonal antibody (a gift from Chugai Pharmaceutical Co. Ltd; Goto et al., 1994) and the rabbit polyclonal BST-2 antibody (Abcam). Other antibodies used were mouse monoclonal antibodies to ezrin (Cell Signaling Technology), myc-9E10 (Sigma-Aldrich), α-tubulin (Sigma-Aldrich), Rac (BD), ZO-1 (Invitrogen), β-actin (Sigma-Aldrich), CD99 (Levy et al., 1979), GFP (Clontech Laboratories, Inc.), and sucrase-isomaltase (a gift from H.-P. Hauri, University of Basel, Basel, Switzerland) and rabbit polyclonal antibodies to β-catenin (Abcam), EBP50 (Abcam), phospho–MLC 2 (Ser19; Cell Signaling Technologies), phospho-ERM (Cell Signaling Technologies), Na^+/K^+ exchanger (Millipore), and RICH2RhoGap (in house). For immunofluorescence, the secondary antibodies used were goat anti–rabbit or mouse Alexa Fluor 488 or Alexa Fluor 594 (Invitrogen) where appropriate. For immunoblotting, the secondary antibodies used were anti–mouse or rabbit HRP linked (Dako). F-actin was labeled with Alexa Fluor 594–phalloidin (Invitrogen), and biotin was labeled with anti-biotin-FITC (Vector Laboratories).

Immunofluorescence and confocal microscopy

Cells were fixed either with methanol or 3.7% PFA, permeabilized with 0.1% Triton X-100, and blocked in 3% BSA/PBS for 1 h. Caco-2 cells were transfected using FuGene (Roche). Clones stably expressing the siRNA were selected with 200 μg/ml hygromycin (Roche), and cells stably expressing siRNA and CD317-GFP were selected with 400 μg G418 (neomycin) as well. Dual immunolabeling was performed by incubating with the primary antibody for 1 h, washing with PBS, and incubating with the relevant Alexa Fluor 594– or Alexa Fluor 488–conjugated secondary antibody for 0.5 h. Fixed cells were imaged using a confocal laser-scanning microscope (TCS-NT; Leica) equipped with a Kr/Ar laser (488-, 594-, and 647-nm lines) attached to an upright epifluorescence microscope (DMRBE; Leica). All images were collected using a 63× NA 1.4 oil immersion objective and processed with Leica and Photoshop (Adobe) software.

SEM

Images were captured as follows. Transwell tissue culture inserts were washed in PBS and fixed in 2% glutaraldehyde (in PBS) at 40°C for at least 16 h. After dehydration through graded ethanol solutions (20 min each in 25, 50, 75, and 100% absolute alcohol). 100–150 μl hexamethyldisilazane (Sigma-Aldrich) was added into each insert and allowed to evaporate (~2 h) in a fume hood. The Transwell membranes were then removed using a scalpel and attached to 12-mm-diameter aluminum SEM stubs (Agar Scientific) using 12-mm-diameter adhesive carbon tabs. The membranes were then gold coated using a sputter coater. The specimens were examined using a scanning electron microscope (501B; Philips), and digital images were acquired on line by analogue to digital conversion using SEM software provided by A. Gebert (Medical School of Hanover, Hanover, Germany; Gebert and Preiss, 1998).

Activated Rac assay

Cells were grown and polarized in 10-cm dishes, washed on ice with PBS, and scraped into lysis buffer (50 mM Tris, pH 7.2, 500 mM NaCl, 10 mM $MgCl_2$, 1% Triton X-100, protease inhibitor cocktail [Roche], and 0.1 mM PMSF). Sepharose beads coupled to a GST–p21-activated kinase–CRIB (i.e., the Rac1/Cdc42-binding domain of p21-activated kinase; Bagrodia et al., 1995) fusion protein were made, and pull-down assays were performed as previously described (Benard and Bokoch, 2002). Proteins were separated by SDS-PAGE, transferred to polyvinylidene fluoride, and probed with an anti-Rac1 antibody.

Membrane and whole cell preparations

Cells were polarized on permeable membranes for 14 d and then treated with nonpenetrating biotinylation reagent EZ-link Sulfo-NHS-biotin (Thermo Fisher Scientific) at 4°C for 30 min on the apical surface. Cells were then fixed and labeled with streptavidin-FITC. Membrane and cytosol fractions were separated by ultracentrifugation (1,000 rpm in a bench-top centrifuge [Eppendorf] at 4°C for 5 min followed by 20 min at 100,000 *g* in an ultracentrifuge [Sorvall]) after cell lysis in a cell cracker (Isobiotec) in hypotonic lysis buffer (10 mM Tris-HCl, pH 7.4, and 10 mM EDTA) with protease inhibitors (Roche). The fractions were probed by immunoblotting with antibodies to RICH2 and CD99. Proteins were separated on 12 or 15% gels, transferred to polyvinylidene fluoride or nitrocellulose, and incubated with primary antibody. Bound primary antibody was detected with HRP-conjugated secondary antibody and chemiluminescence (Roche).

Protein interactions

Bacteriophage display screen. The bacteriophage display library used was a gift from S. Conner and S. Schmid (The Scripps Research Institute, La Jolla, CA). It was constructed using cDNA generated from mRNA isolated from rat brain and screened according to published procedures (Conner and Schmid, 2002). All peptides were synthesized by G. Bloomberg at the University of Bristol's core facility using Fmoc/t-Bu methodology on an automatic peptide synthesizer (Pioneer; Applied Biosystems). Peptides were dissolved in buffer (100 mM Tris-HCl and 100 mM NaCl, pH 7.2) at 2 mg/ml. The bait fusion peptide of the whole rat CD317 cytosolic N terminus was tagged with a hexahistidine sequence at the C terminus: ^{1}MAPSFYHYLPVAMDERWEPKGWSIRR^{27}-H_6 CD317-Ntm-His.

Peptides were also synthesized to preabsorb the phage library before binding to CD317 to limit nonspecific interactions. The C-terminal 27 amino acids of rat TGN38 were synthesized and fused to a hexahistidine tag, and this peptide was used in the first-round phage display screen: H_6-^{314}AFALEGKRSKVTRRPKASDYQRLNLKL^{340} TGN38-Ctm-His.

Peptides were immobilized on Talon Metal Affinity Resin matrix (Clontech Laboratories, Inc.). 5 μl of the phage library was preabsorbed with beads coated with 445 μl TGN38-Ctm-His PBS containing 50 μl of 10× panning buffer (5% [wt/vol] BSA, 250 μg/ml sheared salmon sperm DNA, 5% [wt/vol] NP-40, 250 μg/ml heparin, and 0.05% sodium azide, pH 7.4) for 1 h at room temperature with agitation (modified from Conner and Schmid, 2002). Beads were pelleted, and the supernatant was collected. Approximately 500 μl of the preabsorbed phage library was then incubated for 1 h at room temperature with the immobilized CD317 bait peptide. The CD317-coated beads with bound phage were incubated with

1 ml BLT5403 *Escherichia coli* (in Luria Bertani [LB] broth; OD_{600} = 0.75) in an orbital shaker at 250 rpm at 37°C for ~3 h. The phage infected the bacteria during this incubation. Lytic debris was then cleared by centrifugation (on a bench-top microfuge at 8,000 rpm), and the supernatant was retained for further rounds of biopanning. After four rounds of biopanning using the CD317 bait peptide, the amplified phage supernatant was diluted 10^{-3}–10^{-8}-fold in 100-µl aliquots in LB broth. These were added to 250 µl BLT5403 cells (OD_{600} = 1) and 4 ml of molten 1.6% agarose (<50°C) and overlaid onto LB agar plates. The plates were incubated at 37°C for 1–3 h until individual clear plaques appeared. cDNA inserts were amplified directly from a sample collected from a lytic plaque using the following primers: T7Select forward, 5′-GGAGCTGTCGTATTCCAGTC-3′; and T7Select reverse, 5′-AACCCCTCAAGACCCGTTTAG-3′.

PCR products of different sizes were selected for sequencing. Nucleotide sequences were conceptually translated. The EcoRI restriction enzyme site within the vector sequence defined the reading frame of the downstream peptide sequence; therefore, only open reading frames containing the peptide sequence GDPNS, corresponding to the N-terminal region of the translation, were used in a blastp (protein–protein) BLAST (Basic Local Alignment Search Tool) similarity search against known proteins deposited in the National Center for Biotechnology Information electronic database (http://ncbi.nlm.nih.gov/BLAST).

Pull-down assay. The interaction between putative CD317-interacting proteins and CD317 was studied using a synthetic biotinylated peptide of the whole rat CD317 N-terminal cytosolic domain as shown below. Numbers indicate the amino acids in the full-length CD317 sequence: ^{1}MAPSFYHYLPVAMDERWEPKGWSIRR^{26}-biotin.

The biotin tag was used to immobilize the peptide on streptavidin-coated agarose beads and thereby present the N terminus to interacting proteins in a similar fashion to it protruding from the lipid bilayer. In brief, streptavidin-coated agarose beads were washed three times for 10 min in 5 ml TBS. Beads were harvested by centrifugation in a bench-top centrifuge at 1,000 rpm for 1.5 min. The beads were incubated with TBS containing either 1 mg/ml CD317-Ntm-biotin or 1 mg/ml biotin for 60 min at room temperature. The beads were then washed three times for 10 min in TBS and blocked with 1 mg/ml biotin in TBS at room temperature for 15 min. Again, the beads were washed three times for 10 min. 25-µl aliquots of beads were blocked for nonspecific binding with 3% BSA in resuspension buffer (20 mM Tris-HCl and 100 mM NaCl, pH 7.0) for 30 min at room temperature. Purified recombinant proteins were dialyzed against buffer A (100 mM NaCl, 1 mM $MgCl_2$, and 25 mM Hepes, pH 7.4). 5 mg of whole bacterial cell lysate or 40 µg of dialyzed, purified recombinant proteins were then incubated for 1 h at room temperature with 25 µl of beads before they were washed three times for 10 min in 5 ml of resuspension buffer and purged. At this point, the beads were either snap frozen in liquid nitrogen for storage or were heated to 70°C for 10 min with 20 µl of SDS-PAGE sample buffer (50 mM Tris-HCl, pH 6.8, 4% [wt/vol] SDS, 12% [wt/vol] glycerol, 2 mM EDTA, 0.01% bromophenol blue, and 5% β-mercaptoethanol) to elute any bound protein. The eluted protein was then run on a 12% SDS-PAGE gel and transferred to nitrocellulose for immunoblot analysis using standard protocols.

Surface plasmon resonance (Biacore 3000). The same synthetic biotinylated peptide of the whole cytosolic CD317 N-terminal domain was immobilized on streptavidin-coated sensor chips. The streptavidin-coated chip was loaded with peptide according to the manufacturer's instructions. The Biacore 3000 instrument (GE Healthcare) was prepared with degassed HBS-EP buffer (0.01 M Hepes, pH 7.4, 0.15 M NaCl, 3 mM EDTA, and 0.005% Surfactant P20), and all subsequent solutions were prepared in HBS-EP buffer. All flow rates were maintained at 20 µl/min. 200 µg/ml CD317-Ntm-biotin was bound. Before use, the chips were blocked for nonspecific interactions for 1 min with 3% BSA. Purified recombinant proteins were prepared as before. 1–10-µM concentrations of sample were used at a flow rate of 40 µl/min.

Coimmunoprecipitation. COS cells were transfected with expression plasmids encoding DAMP1-GFP and RICH2-RFP. After 24 h, the cells were washed thoroughly five times in PBS. The cells were then scraped into 2 ml of ice-cold immunoprecipitation buffer (150 mM NaCl, 50 mM Tris-HCl, 5 mM EDTA, pH 7.4, and 1% Triton X-100). 3 mg of protein was diluted in a final volume of 5 ml of immunoprecipitation buffer containing protease inhibitor complex (Roche). Protein G–coated agarose beads were washed twice for 5 min in 10 ml PBS, and the beads were then harvested from solution by centrifuging at 150 *g* for 40 s. 3 mg of preabsorbed lysate was then incubated for 1 h at room temperature with 30 µl of blocked beads and 5 µl anti-GFP (Clontech Laboratories, Inc.), a nonspecific antibody (R26.4C, which detects ZO-1, a membrane-associated nonintegral protein; this antibody was donated by D. Goodenough [Harvard Medical School, Boston, MA]; Stevenson et al., 1986), or no antibody at all. The beads were then pelleted from solution by centrifuging at 150 *g* for 40 s in a bench-top microfuge. Eluted proteins were then separated by SDS-PAGE and transferred to nitrocellulose membrane for immunoblotting with the RICH2 antibody.

For coimmunoprecipitation of endogenous protein, CD317 knockdown and control cells were grown and polarized in 75-cm^2 tissue culture flasks. Cells were washed with ice-cold PBS and then scraped into 2 ml of immunoprecipitation buffer (either 150 mM NaCl, 20 mM Tris, pH 7.5, 10% glycerol, 2% NP-40, 10 mM orthovanadate, protease inhibitor cocktail [Roche], and 200 mM PMSF or 150 mM NaCl, 20 mM Tris, pH 7.5, 10% glycerol, 1% Triton X-100, 10 mM orthovanadate, protease inhibitor cocktail [Roche], and 200 mM PMSF). All reactions were kept on ice. Lysates were centrifuged at 1,000 *g* for 5 min. The lysates were cleared with protein G–Sepharose beads and BSA to 1% for 1 h. The beads were then pelleted at 1,000 *g* for 1 min, and the lysates were incubated with protein G–Sepharose beads coupled to 5 µg of the HM1.24 monoclonal antibody for 4 h. The beads were washed four times with immunoprecipitation buffer, and proteins were eluted by boiling for either 2 min (for the RICH2 antibody) or 10 min (for the EBP50 antibody). Proteins were separated, transferred to nitrocellulose, and probed with either the RICH2 or EBP50 rabbit polyclonal antibody.

Ruffle assays

COS cells were transfected with pRICH2-RFP, pRICH2-A291-RFP, or pEGFP. To induce ruffling, 100 µg/ml PMA was added to media for 5 min. Coverslips were washed with PBS, fixed, and stained with Alexa Fluor 594– or Alexa Fluor 488–phalloidin, and cells were scored +/− for ruffling.

Online supplemental material

Fig. S1 shows that a second CD317 siRNA has the same effect on F-actin distribution in polarized cells as the first and that the phenotype can be rescued by expression of rat CD317. Fig. S2 shows that other CD317 and RICH2 siRNAs have the same biochemical effects as those used in the main paper. Fig. S3 shows that other CD317 and RICH2 siRNAs have the same effects on actin organization and ERM phosphorylation as those used in the main paper. Online supplemental material is available at http://www.jcb.org/cgi/content/full/jcb.200804154/DC1.

We thank Daniel Goodenough, Hans-Peter Hauri, and Chugai Pharmaceuticals Co. Ltd for antibodies, Giles Cory for plasmids, Sean Conner and Sandy Schmid for the bacteriophage display library, and Andreas Gebert for image capture software. We are indebted to Jon Lane, Kate Nobes, and Ash Toye for technical advice and comments on the manuscript.

We thank the Medical Research Council for an Infrastructure Award and Joint Research Equipment Initiative Grant to establish the School of Medical Sciences Cell Imaging Facility.

Submitted: 28 April 2008
Accepted: 10 February 2009

References

Amano, M., H. Mukai, Y. Ono, K. Chihara, T. Matsui, Y. Hamajima, K. Okawa, A. Iwamatsu, and K. Kaibuchi. 1996. Identification of a putative target for Rho as the serine-threonine kinase protein kinase N. *Science*. 271:648–650.

Bagrodia, S., S.J. Taylor, C.L. Creasy, J. Chernoff, and R.A. Cerione. 1995. Identification of a mouse p21 activated kinase. *J. Biol. Chem.* 270:22731–22737.

Bartles, J.R. 2000. Parallel actin bundles and their multiple actin-bundling proteins. *Curr. Opin. Cell Biol.* 12:72–78.

Benard, V., and G.M. Bokoch. 2002. Assay of Cdc42, Rac, and Rho GTPase activation by affinity methods. *Methods Enzymol.* 345:349–359.

Berryman, M. 1993. Ezrin is concentrated in the apical microvilli of a wide variety of epithelial cells whereas moesin is found primarily in endothelial cells. *J. Cell Sci.* 105:1025–1043.

Blasius, A.L., E. Giurisato, M. Cella, R.D. Schreiber, A.S. Shaw, and M. Colonna. 2006. Bone marrow stromal cell antigen 2 is a specific marker of type I IFN-producing cells in the naive mouse, but a promiscuous cell surface antigen following IFN stimulation. *J. Immunol.* 177:3260–3265.

Bretscher, A. 1983. Purification of an 80,000-dalton protein that is a component of the isolated microvillus cytoskeleton, and its localization in nonmuscle cells. *J. Cell Biol.* 97:425–432.

Bretscher, A. 1991. Microfilament structure and function in the cortical cytoskeleton. *Annu. Rev. Cell Biol.* 7:337–374.

Bretscher, A., D. Chambers, R. Nguyen, and D. Reczek. 2000. ERM-Merlin and EBP 50 protein families in plasma membrane organization and function. *Annu. Rev. Cell Dev. Biol.* 16:113–143.

Bretscher, A., K. Edwards, and R.G. Fehon. 2002. ERM proteins and merlin: integrators at the cell cortex. *Nat. Rev. Mol. Cell Biol.* 3:586–599.

Conner, S.D., and S.L. Schmid. 2002. Identification of an adaptor-associated kinase, AAK1, as a regulator of clathrin-mediated endocytosis. *J. Cell Biol.* 156:921–929.

Coso, O.A., M. Chiariello, J.-C. Yu, H. Teramoto, P. Crespo, N. Xu, T. Miki, and J.S. Gutkind. 1995. The small GTP-binding proteins Rac1 and Cdc42 regulate the activity of the JNK/SAPK signaling pathway. *Cell*. 81:1137–1146.

Deborde, S., E. Perret, D. Gravotta, A. Deora, S. Salvarezza, R. Schreiner, and E. Rodriguez-Boulan. 2008. Clathrin is a key regulator of basolateral polarity. *Nature*. 452:719–723.

Delaguillaumie, A., J. Harriague, S. Kohanna, G. Bismuth, E. Rubinstein, M. Seigneuret, and H. Conjeaud. 2004. Tetraspanin CD82 controls the association of cholesterol-dependent microdomains with the actin cytoskeleton in T lymphocytes: relevance to co-stimulation. *J. Cell Sci.* 117:5269–5282.

Denti, M.A., A. Rosa, O. Sthandier, F.G. De Angelis, and I. Bozzoni. 2004. A new vector, based on the PolII promoter of the U1 snRNA gene, for the expression of siRNAs in mammalian cells. *Mol. Ther.* 10:191–199.

Fanning, A.S., and J.M. Anderson. 1999. Protein modules as organizers of membrane structure. *Curr. Opin. Cell Biol.* 11:432–439.

Fölsch, H. 2008. Regulation of membrane trafficking in polarized epithelial cells. *Curr. Opin. Cell Biol.* 20:208–213.

Furuta, B., A. Harada, Y. Kobayashi, K. Takeuchi, T. Kobayashi, and M. Umeda. 2002. Identification and functional characterization of nadrin variants, a novel family of GTPase activating protein for rho GTPases. *J. Neurochem.* 82:1018–1028.

Gebert, A., and G. Preiss. 1998. A simple method for the acquisition of high-quality digital images from analog scanning electron microscopes. *J. Microsc.* 191:297–302.

Goto, T., S.J. Kennel, M. Abe, M. Takishita, M. Kosaka, A. Solomon, and S. Saito. 1994. A novel membrane antigen selectively expressed on terminally differentiated human B cells. *Blood*. 84:1922–1930.

Grasset, E., M. Pinto, E. Dussaulx, A. Zweibaum, and J.F. Desjeux. 1984. Epithelial properties of human colonic carcinoma cell line Caco-2: electrical parameters. *Am. J. Physiol.* 247:C260–267.

Gravotta, D., A. Deora, E. Perret, C. Oyanadel, A. Soza, R. Schreiner, A. Gonzalez, and E. Rodriguez-Boulan. 2007. AP1B sorts basolateral proteins in recycling and biosynthetic routes of MDCK cells. *Proc. Natl. Acad. Sci. USA*. 104:1564–1569.

Haggie, P.M., J.K. Kim, G.L. Lukacs, and A.S. Verkman. 2006. Tracking of quantum dot-labeled CFTR shows near immobilization by C-terminal PDZ interactions. *Mol. Biol. Cell*. 17:4937–4945.

Hall, A. 1998. Rho GTPases and the actin cytoskeleton. *Science*. 279:509–514.

Hannan, L.A., M.P. Lisanti, E. Rodriguez-Boulan, and M. Edidin. 1993. Correctly sorted molecules of a GPI-anchored protein are clustered and immobile when they arrive at the apical surface of MDCK cells. *J. Cell Biol.* 120:353–358.

Hanono, A., D. Garbett, D. Reczek, D.N. Chambers, and A. Bretscher. 2006. EPI64 regulates microvillar subdomains and structure. *J. Cell Biol.* 175:803–813.

Harada, A., B. Furuta, K. Takeuchi, M. Itakura, M. Takahashi, and M. Umeda. 2000. Nadrin, a novel neuron-specific GTPase-activating protein involved in regulated exocytosis. *J. Biol. Chem.* 275:36885–36891.

Hauri, H.P. 1985. Expression and intracellular transport of microvillus membrane hydrolases in human intestinal epithelial cells. *J. Cell Biol.* 101:838–851.

Ishikawa, J., T. Kaisho, H. Tomizawa, B.O. Lee, Y. Kobune, J. Inazawa, K. Oritani, M. Itoh, T. Ochi, K. Ishihara, and T. Hirano. 1995. Molecular cloning and chromosomal mapping of a bone marrow stromal cell surface gene, BST2, that may be involved in pre-B-cell growth. *Genomics*. 26:527–534.

Itoh, T., and M. Fukuda. 2006. Identification of EPI64 as a GTPase-activating protein specific for Rab27A. *J. Biol. Chem.* 281:31823–31831.

Katoh, Y., and M. Katoh. 2004. Identification and characterization of ARHGAP27 gene in silico. *Int. J. Mol. Med.* 14:943–947.

Kupzig, S., V. Korolchuk, R. Rollason, A. Sugden, A. Wilde, and G. Banting. 2003. BST-2/HM1.24 is a raft-associated apical membrane protein with an unusual topology. *Traffic*. 4:694–709.

Kusumi, A., C. Nakada, K. Ritchie, K. Murase, K. Suzuki, H. Murakoshi, R.S. Kasai, J. Kondo, and T. Fujiwara. 2005. Paradigm shift of the plasma membrane concept from the two-dimensional continuum fluid to the partitioned fluid: high-speed single-molecule tracking of membrane molecules. *Annu. Rev. Biophys. Biomol. Struct.* 34:351–378.

Levy, R., J. Dilley, R.I. Fox, and R. Warnke. 1979. A human thymus-leukemia antigen defined by hybridoma monoclonal antibodies. *Proc. Natl. Acad. Sci. USA*. 76:6552–6556.

Neil, S.J., T. Zang, and P.D. Bieniasz. 2008. Tetherin inhibits retrovirus release and is antagonized by HIV-1 Vpu. *Nature*. 451:425–430.

Nijhara, R., P.B. van Hennik, M.L. Gignac, M.J. Kruhlak, P.L. Hordijk, J. Delon, and S. Shaw. 2004. Rac1 mediates collapse of microvilli on chemokine-activated T lymphocytes. *J. Immunol.* 173:4985–4993.

Ohtomo, T., Y. Sugamata, Y. Ozaki, K. Ono, Y. Yoshimura, S. Kawai, Y. Koishihara, S. Ozaki, M. Kosaka, T. Hirano, and M. Tsuchiya. 1999. Molecular cloning and characterization of a surface antigen preferentially overexpressed on multiple myeloma cells. *Biochem. Biophys. Res. Commun.* 258:583–591.

Paladino, S., D. Sarnataro, R. Pillich, S. Tivodar, L. Nitsch, and C. Zurzolo. 2004. Protein oligomerization modulates raft partitioning and apical sorting of GPI-anchored proteins. *J. Cell Biol.* 167:699–709.

Pearson, M.A., D. Reczek, A. Bretscher, and P.A. Karplus. 2000. Structure of the ERM protein moesin reveals the FERM domain fold masked by an extended actin binding tail domain. *Cell*. 101:259–270.

Reczek, D., and A. Bretscher. 2001. Identification of EPI64, a TBC/rabGAP domain-containing microvillar protein that binds to the first PDZ domain of EBP50 and E3KARP. *J. Cell Biol.* 153:191–206.

Richnau, N., and P. Aspenstrom. 2001. Rich, a rho GTPase-activating protein domain-containing protein involved in signaling by Cdc42 and Rac1. *J. Biol. Chem.* 276:35060–35070.

Richnau, N., A. Fransson, K. Farsad, and P. Aspenstrom. 2004. RICH-1 has a BIN/Amphiphysin/Rvsp domain responsible for binding to membrane lipids and tubulation of liposomes. *Biochem. Biophys. Res. Commun.* 320:1034–1042.

Ridley, A.J., and A. Hall. 1992. The small GTP-binding protein rho regulates the assembly of focal adhesions and actin stress fibers in response to growth factors. *Cell*. 70:389–399.

Ridley, A.J., H.F. Paterson, C.L. Johnston, D. Diekmann, and A. Hall. 1992. The small GTP-binding protein rac regulates growth factor-induced membrane ruffling. *Cell*. 70:401–410.

Rodriguez-Boulan, E., and A. Müsch. 2005. Protein sorting in the Golgi complex: shifting paradigms. *Biochim. Biophys. Acta*. 1744:455–464.

Rollason, R., V. Korolchuk, C. Hamilton, P. Schu, and G. Banting. 2007. Clathrin-mediated endocytosis of a lipid-raft-associated protein is mediated through a dual tyrosine motif. *J. Cell Sci.* 120:3850–3858.

Saotome, I., M. Curto, and A.I. McClatchey. 2004. Ezrin is essential for epithelial organization and villus morphogenesis in the developing intestine. *Dev. Cell*. 6:855–864.

Sargiacomo, M., M. Lisanti, L. Graeve, A. Le Bivic, and E. Rodriguez-Boulan. 1989. Integral and peripheral protein composition of the apical and basolateral membrane domains in MDCK cells. *J. Membr. Biol.* 107:277–286.

Schuck, S., and K. Simons. 2004. Polarized sorting in epithelial cells: raft clustering and the biogenesis of the apical membrane. *J. Cell Sci.* 117:5955–5964.

Sheetz, M.P. 1983. Membrane skeletal dynamics: role in modulation of red cell deformability, mobility of transmembrane proteins, and shape. *Semin. Hematol.* 20:175–188.

Simons, K., and D. Toomre. 2000. Lipid rafts and signal transduction. *Nat. Rev. Mol. Cell Biol.* 1:31–39.

Songyang, Z., S.E. Shoelson, M. Chaudhuri, G. Gish, T. Pawson, W.G. Haser, F. King, T. Roberts, S. Ratnofsky, R.J. Lechleider, et al. 1993. SH2 domains recognize specific phosphopeptide sequences. *Cell*. 72:767–778.

Stevenson, B.R., J.D. Siliciano, M.S. Mooseker, and D.A. Goodenough. 1986. Identification of ZO-1: a high molecular weight polypeptide associated with the tight junction (zonula occludens) in a variety of epithelia. *J. Cell Biol.* 103:755–766.

Tapon, N., and A. Hall. 1997. Rho, Rac and Cdc42 GTPases regulate the organization of the actin cytoskeleton. *Curr. Opin. Cell Biol.* 9:86–92.

Toye, A.M., R.C. Williamson, M. Khanfar, B. Bader-Meunier, T. Cynober, M. Thibault, G. Tchernia, M. Dechaux, J. Delaunay, and L.J. Bruce. 2008. Band 3 Courcouronnes (Ser667Phe): a trafficking mutant differentially rescued by wild type band 3 and glycophorin A. *Blood*. 111:5380–5389.

Van Damme, N., G. Goff, C. Katsura, R.L. Jorgenson, R. Mitchell, M.C. Johnson, E.B. Stephens, and J. Guatelli. 2008. The interferon-induced protein BST-2 restricts HIV-1 release and is downregulated from the cell surface by the viral Vpu protein. *Cell Host Microbe*. 3:245–252.

Vidal-Laliena, M., X. Romero, S. March, V. Requena, J. Petriz, and P. Engel. 2005. Characterization of antibodies submitted to the B cell section of

the 8th Human Leukocyte Differentiation Antigens Workshop by flow cytometry and immunohistochemistry. *Cell. Immunol.* 236:6–16.

Viola, A., and N. Gupta. 2007. Tether and trap: regulation of membrane-raft dynamics by actin-binding proteins. *Nat. Rev. Immunol.* 7:889–896.

Weinman, E.J., D. Steplock, Y. Wang, and S. Shenolikar. 1995. Characterization of a protein cofactor that mediates protein kinase A regulation of the renal brush border membrane Na(+)-H+ exchanger. *J. Clin. Invest.* 95:2143–2149.

Wells, C.D., J.P. Fawcett, A. Traweger, Y. Yamanaka, M. Goudreault, K. Elder, S. Kulkarni, G. Gish, C. Virag, and C. Lim. 2006. A Rich1/Amot complex regulates the Cdc42 GTPase and apical-polarity proteins in epithelial cells. *Cell.* 125:535–548.

Yeaman, C., K.K. Grindstaff, and W.J. Nelson. 1999. New perspectives on mechanisms involved in generating epithelial cell polarity. *Physiol. Rev.* 79:73–98.

Yonemura, S., S. Tsukita, and S. Tsukita. 1999. Direct involvement of ezrin/radixin/moesin (ERM)-binding membrane proteins in the organization of microvilli in collaboration with activated ERM proteins. *J. Cell Biol.* 145:1497–1509.